Supratransmission phenomenon in a Fermi-Pasta-Ulam diatomic lattice

Christian Simadji Ngamou,[*] Frank Thomas Ndjomatchoua [⬡],[†] Michael Mekontchou Foudjio [⬡],[‡]
Carlos Lawrence Gninzanlong [⬡],[§] and Clément Tchawoua[‖]

Department of Physics, Faculty of Science, University of Yaoundé 1, P.O. Box 812, Yaoundé, Cameroon

The nonlinear supratransmission phenomenon in a Fermi-Pasta-Ulam (FPU) diatomic lattice with two forbidden bands is investigated. Using a decoupling ansatz for the motion of the two different sublattices combined with the continuum (quasidiscrete) approximation, we derived analytically the threshold amplitudes of supratransmission occurrence when a sinusoidal driving with frequency in the upper forbidden band (lower forbidden band gap between acoustic and optical modes) is applied at one end. The resulting estimate of the threshold of a lattice with a first heavy particle is different to the one obtained from a lattice with a first light particle, showing the influence of the driven particle and giving also the possibility to have two thresholds on each forbidden gap of a diatomic lattice by switching the order of light (m) and heavy (M) masses. In the lower forbidden band, the dependence of the supratransmission threshold on the mass ratio ($\mu = m/M$) has been evidenced and it appears that for large (small) values of μ, that is $\mu > 60\%$, the coupling between the two modes must (must not) be considered. Numerical explorations were subsequently performed with an emphasis on the dependence of the threshold on the driving frequency and also on the mass of the driven particle (light or heavy). A good agreement is found between the numerical and analytical thresholds. For the limit case where all the masses are identical, the results of the monoatomic FPU previously found in the literature are recovered.

I. INTRODUCTION

The study of spatially periodic structures is an emerging discipline that lies at the crossroads of vibration and acoustics engineering and condensed matter physics [1–3]. Such structures exhibit rich dynamic characteristics, contributing to their diverse applications in a wide range of physical systems, including phononic crystals and acoustic metamaterials [1], as well as photonic lattice materials [4]. Although most systems encountered in nature are monoatomic [1,4,5], a complex setup with more than one elementary constituent in the unit cell can also form lattice structures. Granular crystals [6,7], chains of coupled pendulums [8] and electrical transmission lines [9–11] are illustrative cases for diatomic lattices.

Since the celebrated Fermi-Pasta-Ulam (FPU) first numerical experiment in 1954 [12], anharmonic oscillator chains have become powerful tools in dealing with both fundamental aspects of statistical physics and nonlinear wave phenomena [13], at the same time serving as the simplest prototypes for extremely complex condensed matter systems [13]. The diatomic version of the FPU model will be used as the core model of this study.

———
[*]Corresponding author: christthichi@gmail.com
[†]Corresponding author: ftndjomatchoua@gmail.com
[‡]michaelmekontchou@gmail.com
[§]gcarloslawrence@yahoo.fr
[‖]Corresponding author: ctchawa@yahoo.fr

For motions with small amplitudes (linear operating range), the dynamic response of periodic structures is very well understood [14]. The wave-filtering properties of one-dimensional periodic structures are of paramount relevance in engineering applications: for an exactly periodic structure with no damping, the structure behaves as a frequency filter. Waves with frequency components within particular intervals (known as pass bands) travel through the structure unattenuated, whereas all other frequency components in the forbidden band gap are spatially attenuated as they propagate through the structure. For a diatomic lattice, the phonon spectrum of the system consists of two branches (acoustic and optical ones), induced by the mass or force-constant difference of two kinds of particles [14]. Due to nonlinearity, gap modes may appear as localized excitations with the vibrating frequency falling within the prohibited frequency range of the linear spectrum [6,15–17].

More interestingly, it was demonstrated that nonlinear chains sinusoidally driven at their boundaries can propagate energy in the forbidden frequency band gap [18]. In this case, energy transmission occurs above a precise (frequency-dependent) threshold amplitude and occurs in the form of nonlinear localized modes (gap solitons) [18]. The phenomenon occurs in diverse physical systems such as mechanical [18], electrical [19], and optical lattices [20] (just to mention a few).

Supratransmission has been observed in a variety of complex spatially discrete structures, including disordered [21], structures with on-site potential [22,23], two-dimensional [24], and transversely coupled [25–27] lattices. Surprisingly,

supratransmission in diatomic anharmonic one-dimensional systems is rarely studied (but see Refs. [28,29]), despite the fact that realistic diatomic models have a wide range of applications [6–11]. In the present study, we aim to extend the monoatomic studies of supratransmission on the FPU lattice [30,31] and consider a diatomic version that exhibits two modes (acoustic and optical) and two forbidden frequency band gaps.

Due to the complexity of the system, methods based on an asymptotic solution obtained by decoupling *ansatz* [32–36], and quasidiscrete approximation [37] which provides an accurate nonlinear supratransmission threshold (NST) prediction are used here. These methods are restricted to neither the specific case of second harmonic generation nor to the quadratic nature of the nonlinearity [32–36]. Moreover, they can be applied to a wide class of nonintegrable discrete nonlinear systems since they do not require known analytical expressions for their solutions. These methods thus furnishe a practical tool highly interesting for further applications in any multiatomic system.

To achieve the objectives of this study, the Sec. II is devoted to description of the dynamics of particles under the nonlinear potential and the derivation of analytical threshold of supratransmission. Section III explores numerically the phenomenon and the case of a lattice with the lighter particle at the first range; the results are discussed in Sec. IV, and a conclusion is presented in Sec. V.

II. THE MODEL

The model under consideration is a Fermi-Pasta-Ulam (FPU) diatomic chain, where the light and heavy particles have, respectively, the mass m and M ($m < M$). The Hamiltonian function of the system is given by

$$H = \sum_j \left[\frac{1}{2} \mathcal{M}_j \left(\frac{du_j}{dt} \right)^2 + \phi(u_{j+1} - u_j) \right], \quad (1)$$

where $\phi(r) = \frac{1}{2}K_2 r^2 + \frac{1}{4}K_4 r^4$, K_2, and K_4 are positive constants representing harmonic and quartic potentials, respectively, u_j is the displacement from the equilibrium position of the jth particle with the mass $\mathcal{M}_j = M\delta_{j,2l} + m\delta_{j,2l+1}$ ($\delta_{j,s}$ is the Kronecker's δ which has the values 0 for $j \neq s$ and 1 otherwise; l is an integer) and $u_j = V_j \delta_{j,2l} + W_j \delta_{j,2l+1}$. The derived equations of motion of the light and heavy particles are given by

$$\ddot{V}_n = J_2(W_n + W_{n-1} - 2V_n) + J_4[(W_n - V_n)^3 - (V_n - W_{n-1})^3], \quad (2)$$

$$\ddot{W}_n = I_2(V_{n+1} + V_n - 2W_n) + I_4[(V_{n+1} - W_n)^3 - (W_n - V_n)^3], \quad (3)$$

where $I_2 = K_2/m$, $J_2 = K_2/M$, $I_4 = K_4/m$, and $J_4 = K_4/M$.

Taking the linear form of Eqs. (2) and (3) and seeking plane wave solutions under the form $V_n(t) = V_0 \exp[i(2knD - \omega t)]$ and $W_n(t) = W_0 \exp[i(2knD - \omega t)]$, where $i^2 = -1$, k being the wave vector and ω the phonon frequency; the estimated
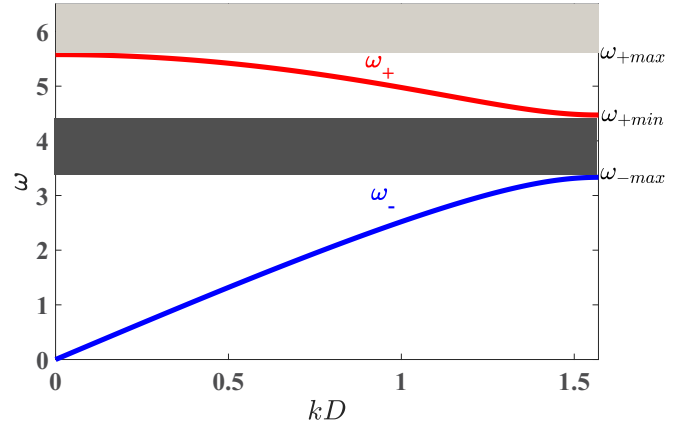

FIG. 1. Linear dispersion relation. Blue and red curves represent acoustic and optical modes respectively; $K_2 = 1$, $K_4 = 1$, $m = 0.1$, $M = 0.18$.

linear dispersion law is

$$\omega_\pm(k) = \sqrt{I_2(1 + \mu) \pm I_2\sqrt{2\mu \cos(2kD) + 1 + \mu^2}}, \quad (4)$$

where $\mu = m/M$.

The minus (plus) sign corresponds to the acoustic (optical) modes [14] and D is the lattice spacing. Equation (4) is represented in Fig. 1. The two forbidden bands gaps, between acoustic and optical modes (dark gray band: $\omega \in]\omega_{-max}, \omega_{+min}[$), and above the optical mode (light gray band: $\omega \in]\omega_{+max}, +\infty[$), are displayed in Fig. 1. Here, $\omega_{-max} = \sqrt{2J_2}$, $\omega_{+min} = \sqrt{2I_2}$, and $\omega_{+max} = \sqrt{2I_2(1 + \mu)}$. When the driving frequency lies inside the forbidden bands, the wave is expected to decay [14], whereas, in a nonlinear lattice, when the driving amplitude is greater than a certain value, the wave can persist [18–21,24–26,28,29]. Our purpose is to prove the existence of this values through analytical and numerical means for the diatomic β-FPU lattice.

A. Supratransmission threshold in upper forbidden band

The upper forbidden band is bounded on the top at $k = 0$, and thus the long wave-length limit can be considered. In this consideration, and with the slowly varying envelope hypothesis (in space and time), the approximations $x = 2nD$, $u_n(t) = u(x, t)$, $u_{n\pm1}(t) = u(x \pm 2D, t)$ are assumed. However, due to the different nature of particles of the two sublattices which impose a discontinuity to the overall movement, the continuum limit is applied only to each type of particles separately. In this configuration, the Taylor series expansion of $u(x \pm 2D, t)$ is given by

$$u(x \pm 2D, t) = \sum_{l=1}^{4} \frac{(\pm 2D)^l}{l!} \partial_x^l u(x, t) + \mathcal{O}(D^5). \quad (5)$$

By using the decoupling ansatz method [33,36] we can approximate W as

$$W = \lambda_j \left[V + \sum_{l=1}^{4} b_{l,j} \frac{D^l}{l!} \partial_x^l V \right] + \mathcal{O}(D^5), \quad (6)$$

where $\partial_x V = \partial V / \partial x = V_x$; λ_j, $b_{l,j}$ are constants which are determined by replacing Eq. (5) in Eqs. (2) and (3) and thereafter inserting into the resulting equations the expression of W given by Eq. (6).

The two resulting equations should be identical and being so, we obtain two possible values for λ_j namely: $\lambda_1 = 1$ and $\lambda_2 = -1/\mu$, corresponding to acoustic and optical mode respectively, and as in Refs. [33,36] the value of the coefficients b_j for each mode. For the optical mode ($\lambda = -1/\mu$) which is of interest in this subsection, terms up to $\mathcal{O}(D^3)$ are considered, and the coefficients are given by

$$b_1 = 1, \quad b_2 = \frac{2\mu}{1+\mu}, \quad b_3 = b_4 = 0. \tag{7}$$

In the forbidden bands, there are two different behaviors of vibrating particles, depending on the proximity of the driving frequency with the acoustic or the optical mode: when the driving frequency is taken within the upper forbidden gap, the particles behavior is that of optical mode and when the driving frequency is taken within the lower forbidden band gap, the particles behavior is ordered by the band width.

Inserting in Eqs. (2) and (3) the Taylor expansion Eq. (5) and the decoupling ansatz procedure Eq. (6) with the previous values of its coefficient, we obtain when keeping only terms up to $\mathcal{O}(\epsilon^3)$ the following equation:

$$V_{tt} + cV_{xx} + dV + qV^3 = 0, \tag{8}$$

where

$$c = \frac{2J_2 D^2}{1+\mu}, \quad d = 2I_2(1+\mu), \quad q = \frac{2J_4(1+\mu)^3}{\mu^3}.$$

Taking the linear form of Eq. (8) and looking for plane wave solutions on the form $V = V_0 \exp[i(kx - \Omega t)]$, the linear dispersion relation $\Omega^2 = d - ck^2$ can be derived. Since the pulse soliton solution is needed, the case $d > 0$ is considered. By taking the variable V on the form [33,36]

$$V(x,t) = \Phi(x,t) \exp[i(kx - \omega t)] + \text{c.c.}, \tag{9}$$

(c.c. being the complex conjugate of the first term and $i^2 = -1$) and using the new variables $\eta = x - v_g t$ and $\tau = \epsilon t$, we derive the nonlinear Schrödinger equation

$$-i\Phi_\tau + P\Phi_{\eta\eta} + Q|\Phi|^2\Phi = 0, \tag{10}$$

where

$$P = -\frac{v}{2}, \quad Q = \frac{3q}{2\omega}, \quad \text{and } v = \frac{d^2\omega}{dk^2} = -\frac{v_g^2 + c}{\omega}.$$

We obtain when seeking solutions of Eq. (10) as static breather solutions on the form $\Phi(\eta, \tau) = A(\eta) \exp(-i\omega_s \tau)$, where $\omega_s = \omega - \omega_{+\text{max}}$ for the upper forbidden band:

$$\Phi(\eta, \tau) = \sqrt{\frac{2\omega_s}{Q}} \, \text{sech}\left(\pm \sqrt{\frac{\omega_s}{P}} (\eta - \eta_0) \right) \exp(-i\omega_s \tau). \tag{11}$$

Following the analytical procedure in Refs. [19,23], the supratransmission threshold is given by

$$A_{\text{th}} = \sqrt{\frac{8(\omega - \omega_{+\text{max}})}{Q}}, $$

and it takes the final form

$$A_{\text{th}_{\text{up}}} = \sqrt{\frac{8\omega\mu^3(\omega - \omega_{+\text{max}})}{3J_4(1+\mu)^3}}. \tag{12}$$

B. Supratransmission threshold in the lower forbidden band

The lower forbidden band, as we can see on Fig. 1, is bounded at $k = \frac{\pi}{2D}$, and for this value of wave number, the long wave-length limit and then the decoupling ansatz given in Eq. (6) are no longer valid.

A more general form of the decoupling ansatz method for arbitrary wave-length is described in Ref. [34]. To perform this, we seek solutions of Eqs. (2) and (3) on the form

$$
\begin{aligned}
V_n &= A_n e^{i(2knD - \omega t)} + \text{c.c.}, \\
W_n &= B_n e^{i(2knD - \omega t)} + \text{c.c.},
\end{aligned} \tag{13}
$$

and assumed the continuum approximation $2nD \to x$ so that $A_n(t) \to A(x,t)$ and $B_n(t) \to B(x,t)$. After the Taylor expansion of A_{n+1} and B_{n-1} around the continuum variables $A(x,t)$ and $B(x,t)$ respectively, we can apply the decoupling ansatz:

$$B(x,t) = \sigma e^{ikD}\left(A + b_1 DA_x + \frac{b_2}{2}DA_{xx} + b_3 DA_{xt} + b_0|A|^2A \right), \tag{14}$$

which gives for $k = \frac{\pi}{2D}$ two possible values of σ namely $\sigma = 0$ and $\sigma = -\infty$. The last value of σ which is obtained for optical mode renders a divergence and only the former ($\sigma = 0$) obtained for acoustic mode can be used to derive the coefficients b_1, b_2, b_3 and b_0 given in Ref. [34] and thereafter V_n and W_n as

$$
\begin{aligned}
V_n &= (-1)^n A e^{-i\omega t} + \text{c.c.}, \\
W_n &= 0.
\end{aligned} \tag{15}
$$

Following the procedure described in Ref. [34], we obtain the nonlinear Schrödinger equation which is given for $\sigma = 0$ and $k = \frac{\pi}{2D}$ by

$$-iA_\tau + P_a A_{\eta\eta} + Q_a|A|^2A = 0, \tag{16}$$

where

$$P_a = \frac{\sqrt{2J_2}D^2}{1 - \mu} \quad \text{and} \quad Q_a = \frac{3J_4}{\omega_{-\text{max}}}.$$

Equation (16) is similar to that obtained in Sec. II A and its static solution (with $\omega_s = \omega - \omega_{-\text{max}}$) can be written as

$$A(\eta, \tau) = \sqrt{\frac{2\omega_s}{Q_a}} \, \text{sech}\left(\pm \sqrt{\frac{\omega_s}{P_a}} (\eta - \eta_0) \right) \exp(-i\omega_s \tau). \tag{17}$$

Thus,

$$V(\eta, \tau) = \sqrt{\frac{2\omega_s}{Q_a}} \, \text{sech}\left(\pm \sqrt{\frac{\omega_s}{P_a}} (\eta - \eta_0) \right) e^{(-i\omega_s \tau)} e^{i\theta} + \text{c.c.}, \tag{18}$$

and the supratransmission threshold is given by

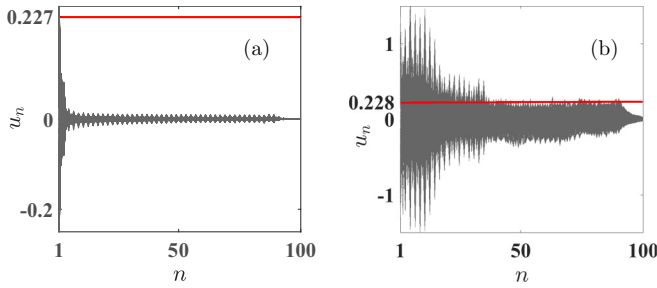$$A_{\text{th}_{\text{low}_1}} = \sqrt{\frac{8\omega_{-\text{max}}(\omega - \omega_{-\text{max}})}{3J_4}}. \tag{19}$$

FIG. 2. Spatial evolution of plane wave within the chain for driving amplitude $A = 0.227$ (a) and $A = 0.228$ (b); $\omega = 6.0$, $m = 0.1$, $M = 0.18$; red line stands for the driving amplitude value.
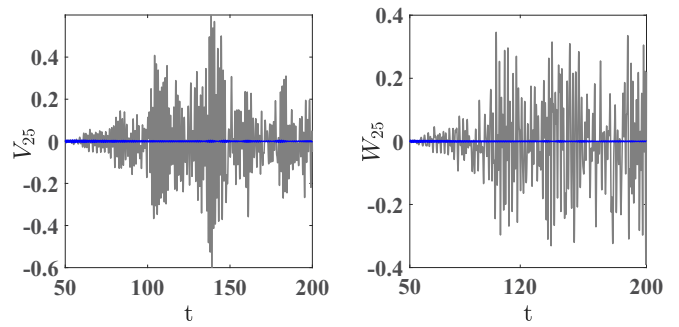

FIG. 3. Behavior of the particles V_{25} and W_{25} for the insulating regime $A = 0.227$ (blue curves) and propagating regime $A = 0.228$ (gray curves), $\omega = 6.0$, $K_2 = 1$, $K_4 = 1$, $m = 0.1$, $M = 0.18$.

III. NUMERICAL SIMULATIONS

In this part, we deal to find numerically the supratransmission thresholds in the two forbidden bands and thereafter to compare with their analytical analogs found in Sec. II.

For the numerical simulations, a lattice of 100 particles is considered where the masses of light and heavy particles are initially fixed at $m = 0.1$ and $M = 0.18$, respectively. With these values of m and M, the lower and the upper band gap are located in]3.333, 4.472[and]5.578, $+\infty$[, respectively. The first particle (of mass M) is subjected to a periodic excitation $V_0(t) = A \cos(\omega t)$ which frequency ω lied within the upper or lower forbidden band gap frequency while the remaining particles of the chain being initially at rest. Throughout the section, we shall use the parameter $D = 1$. To avoid initial shocks formation, the external driver is modified as $V_0(t) = A[1 - \exp(-t/\tau)] \cos(\omega t)$, with $\tau = 5$. To avoid the reflections at the boundary of the lattice, the 10 last particles are submitted to a dissipation with a damping coefficient value $\gamma = 5$. The brute-force method combined with the bisection search is applied to determine the supratransmission threshold numerically [23]. To do this, the interval of driving amplitude leading to the wave propagation although the external driving frequency lied in the forbidden band is identified using a brute-force procedure. Once this interval is found, it is subsequently refined through a bisection search algorithm and stopped when the precision of 10^{-6} is reached. The system is numerically integrated by using the fifth-order Runge-Kutta formula with a fixed time step $\Delta t = 10^{-3}$. The supratransmission is assumed to occur (stopping criterion of the algorithm) as soon as $\max[u_{50}(t)]$ is above the driving amplitude A. To detect the onset of the supratransmission, the spatial evolution of $u_n(t)$ and the behavior of particles $n = 50$ and $n = 51$ are monitored. The onset of supratransmission can also be detected by evaluating the energy flux density as indicated in Refs. [30,38,39].

A. Upper forbidden band gap frequencies

We consider the given periodic excitation with driving frequency $\omega = 6.0$ and for two different values of driving amplitude ($A = 0.227$ and $A = 0.228$).

A sudden propagation of the wave in the system for the case $A = 0.228$ can be observed (Fig. 2). Thus, $A = 0.228$

corresponds to the threshold amplitude of the supratransmission phenomenon occurrence. This observation is confirmed by the behavior of particles V_{25} and W_{25} for the two values of driving amplitude displayed on Fig. 3. We can observe a significant amplification of the driving amplitude when pass from $A = 0.227 < A_{\text{th}}$ to $A = 0.228 = A_{\text{th}}$. It can be noticed that a slight increase of 0.1% is enough to trigger the propagation of the incident wave along the lattice although ω is in the forbidden band gap.

The numerical and analytical thresholds as a function of driving frequency for three values of the parameter couples (m, M) [(0.1, 0.18), (0.3, 0.5), (1, 1.5)] which correspond to mass ratio of 55%, 60%, and 66%, respectively, are monitored.

Figure 4 shows a good agreement between analytical supratransmission threshold and its numerical analog. The increase of mass ratio m/M induces a net increases of the threshold, while the threshold always increases with the values of forbidden band gap frequencies.
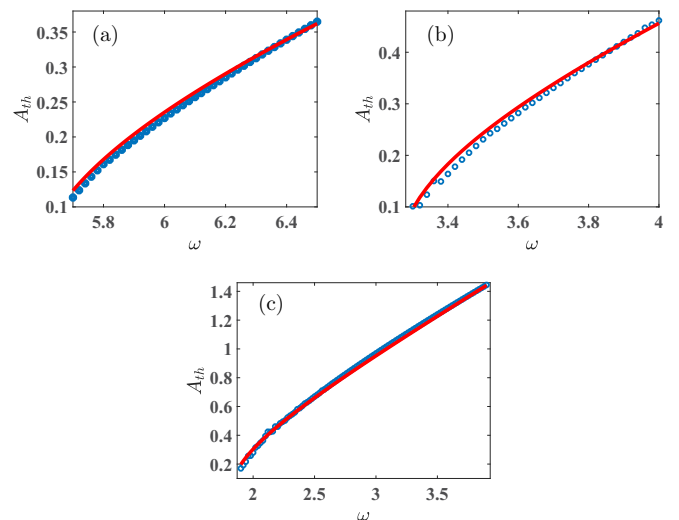

FIG. 4. Threshold amplitude versus the driving frequency. Numerical (blue circles) and analytical (red solid lines) for (m, M) taking the values (0.1, 0.18) (a); (0.3, 0.5) (b); and (1, 1.5) (c); $K_2 = 1$, $K_4 = 1$, $D = 1$.
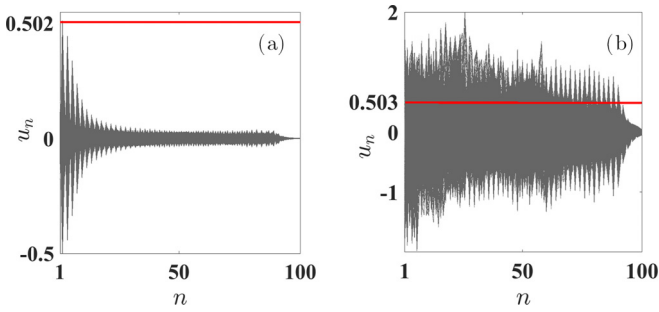
FIG. 5. Spatial evolution of plane wave for (a) $A = 0.502$ and (b) $A = 0.503$; $\omega = 3.5$, $K_2 = 1$, $K_4 = 1$, $m = 0.1$, $M = 0.18$; red lines stand for the driving amplitude values.

B. Lower forbidden band gap frequencies

Submitting the lattice to the same periodic excitation as in upper forbidden band, with a driving frequency $\omega = 3.5$, the supratransmission phenomenon is noticed as a sudden transmission when slightly varying the driving amplitude from $A = 0.502$ to $A = 0.503$ [Fig. 5]. The behavior of particles V_{25} and W_{25} shown in Fig. 6 confirms the value of the supratranmission threshold.

For three couples of parameters (m, M): (0.1, 0.18), (0.3, 0.5), and (1, 1.5), the numerical threshold amplitude as a function of driving frequency is plotted along with its analytical analog Eq. (19). The increase of the mass ratio m/M induces a net decrease of the threshold, while the threshold always increases with the values of forbidden band gap frequencies. On Fig. 7, a good agreement is observed between the numerical and the analytical threshold Eq. (19) as the frequencies increase in the lower forbidden band. From Fig. 7, we can also deduct that the analytical thresholds are more accurate for lower values of the mass ratio m/M. A growing disagreement can be noticed when the mass ratio increases beyond 60%; the analytical procedure has to be reviewed for these values.

C. Effect of the coupled modes on the supratransmission threshold

The study of threshold with respect to driving frequency in lower forbidden band revealed a disagreement between numerical and analytical results as the mass threshold ratio m/M increases. We can also notice that when this ratio increases,
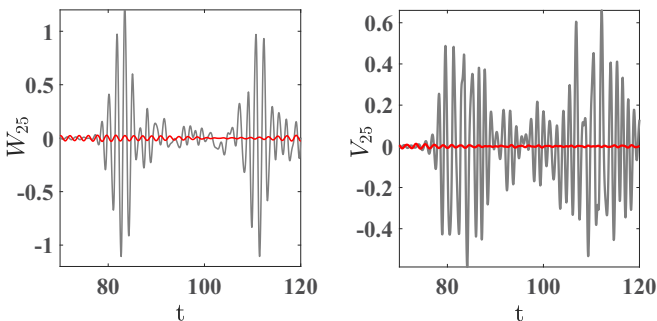

FIG. 6. Behavior of the particles V_{25} and W_{25} for the insulating regime $A = 0.502$ (red curves) and propagating regime $A = 0.503$ (gray curves); $\omega = 3.5$, $K_2 = 1$, $K_4 = 1$, $m = 0.1$, $M = 0.18$.
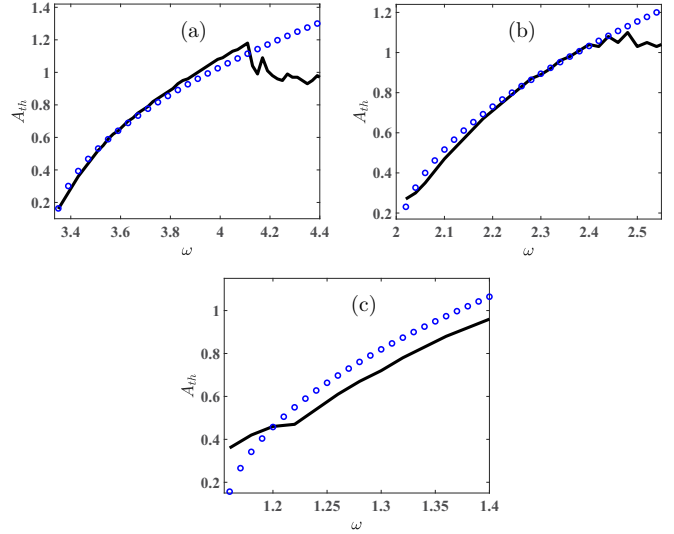

FIG. 7. Threshold amplitude versus driving frequency. Numerical results (gray solid line) and analytical threshold (blue circles) for (m, M) taking the values (0.1, 0.18) (a), (0.3, 0.5) (b), and (1, 1.5) (c); $K_2 = 1$, $K_4 = 1$, $D = 1$.

the width of lower forbidden band decreases. A narrow band gap frequencies, which suppose a great proximity between the upper and the lower cutoff frequency of the acoustic and optical mode respectively results in a coupling between these two modes [37]. The seeking of Coupled modes static breathers shall be necessary to investigate the supratransmission phenomenon in lower forbidden band for narrow band gap frequencies.

We consider the following asymptotic expansion for V_n and W_n [37]:

$$
\begin{aligned}
V_n &= \epsilon V_{n,n}^{(1)} + \epsilon^2 V_{n,n}^{(2)} + \epsilon^3 V_{n,n}^{(3)} + ..., \\
W_n &= \epsilon W_{n,n}^{(1)} + \epsilon^2 W_{n,n}^{(2)} + \epsilon^3 W_{n,n}^{(3)} + ...
\end{aligned}
\tag{20}
$$

The quasidiscrete approximation has early been study by Hu *et al.* [37], for a diatomic FPU lattice. Following this procedure, we consider the slow variables:

$$
\begin{aligned}
\eta &= \epsilon\left(nD - v_g t\right), \\
\tau &= \epsilon^2 t,
\end{aligned}
\tag{21}
$$

and the fast variable

$$
\Phi_n(t) = 2knD - \omega t. \tag{22}
$$

When inserting Eq. (20) into Eqs. (2) and (3), and taking into account Eqs. (21) and (22), we derive $V_{n,n}^{(1)}$ and $W_{n,n}^{(1)}$ from the leading order (ϵ^1), at the limit $k = \frac{\pi}{2D}$ of the first Brillouin zone as

$$
\begin{aligned}
V_{n,n}^{(1)} &= (-1)^n A_{11}(\eta, \tau) \exp(-i\omega_{-\max}t) + \text{c.c.}, \\
W_{n,n}^{(1)} &= (-1)^n B_{11}(\eta, \tau) \exp(-i\omega_{+\min}t) + \text{c.c.}
\end{aligned}
\tag{23}
$$

At the second order (ϵ^2), the solvability conditions yield $v_g = 0$; and at the third order (ϵ^3) we derived when taking

into account Eq. (23) and the solvability conditions obtained from the second order, the following coupled equations:

$$i\frac{\partial}{\partial\tau}A_{11} - \frac{K_2^2 D^2}{2Mm\omega_{-\max}(\omega_{+\min}^2 - \omega_{-\max}^2)}\frac{\partial^2}{\partial\eta^2}A_{11}$$
$$-\frac{3K_4}{M\omega_{-\max}}(|A_{11}|^2 + 2|B_{11}|^2)A_{11} = 0, \qquad (24)$$

$$i\frac{\partial}{\partial\tau}B_{11} - \frac{K_2^2 D^2}{2Mm\omega_{+\min}(\omega_{-\max}^2 - \omega_{+\min}^2)}\frac{\partial^2}{\partial\eta^2}B_{11}$$
$$-\frac{3K_4}{m\omega_{+\min}}(|B_{11}|^2 + 2|A_{11}|^2)B_{11} = 0. \qquad (25)$$

When using the new variables $\Phi = \epsilon A_{11}$ and $\Psi = \epsilon B_{11}$ into Eqs. (24) and (25), we obtain simpler forms depending to the initial variables x_n and t

$$i\frac{\partial}{\partial t}\Phi - P_1\frac{\partial^2}{\partial x_n^2}\Phi - Q_1(|\Phi|^2 + 2|\Psi|^2)\Phi = 0,$$
$$\qquad (26)$$
$$i\frac{\partial}{\partial t}\Psi - P_2\frac{\partial^2}{\partial x_n^2}\Psi - Q_2(|\Psi|^2 + 2|\Phi|^2)\Psi = 0,$$

where

$$P_1 = \frac{K_2 J_2 D^2}{4\omega_{-\max}(1-\mu)}, \quad P_2 = -\frac{K_2 J_2 D^2}{4\omega_{+\min}(1-\mu)},$$
$$Q_1 = \frac{3\omega_{-\max}J_4}{2J_2}, \quad Q_2 = \frac{3\omega_{+\min}J_4}{2J_2}.$$

1. Band with negligible coupling

Since we are at the limit $k = \frac{\pi}{2D}$ we can do the approximation $\Psi = 0$ for the acoustic mode and $\Phi = 0$ for the optical mode (see Sec. II); we thus obtain for each case a nonlinear Schrödinger equation

$$i\frac{\partial}{\partial t}\Phi - P_1\frac{\partial^2}{\partial x_n^2}\Phi - Q_1|\Phi|^2\Phi = 0, \qquad (27)$$

$$i\frac{\partial}{\partial t}\Psi - P_2\frac{\partial^2}{\partial x_n^2}\Psi - Q_2|\Psi|^2\Psi = 0. \qquad (28)$$

Based on the *PQ* product, only Eq. (27) allows static breather solutions. The solutions of Eq. (28) shall not be discussed in this work.

When seeking solution of Eq. (27) on the for $\Phi = a(\eta)e^{-i\omega_s t}$ and following the same procedure as in Sec. II, we obtain a static breather solution of acoustic mode

$$\Phi(x_n, t) = \sqrt{\frac{2\omega_s}{Q_1}} \text{sech}\left(\pm\sqrt{\frac{\omega_s}{P_1}}(x_n - x_0)\right)\exp(-i\omega_s t),$$
$$\qquad (29)$$

where $\omega_s = \omega - \omega_{-\max}$.

Thereafter, we derived the supratransmission threshold

$$A_{th_{low_3}} = \sqrt{\frac{8\omega_{-\max}(\omega - \omega_{-\max})}{3J_4}}. \qquad (30)$$

We can note that the threshold Eq. (30) obtained for acoustic mode excitation is identical to the threshold Eq. (19) early obtained in Sec. II.
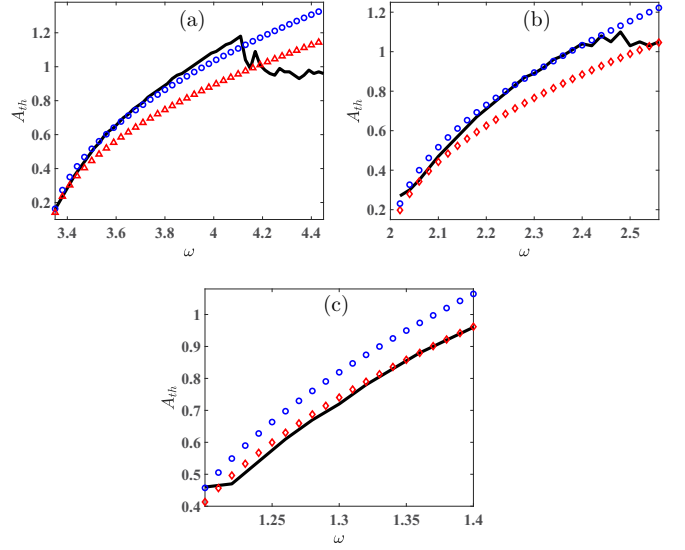

FIG. 8. Threshold amplitude versus the driving frequency. Numerical (black solid lines) and analytical thresholds $A_{th_{low3}}$ (blue circles) and $A_{th_{low4}}$ (red diamonds) for (m, M) taking the values (0.1,0.18) (a); (0.3,0.5) (b); and (1,1.5) (c); $K_2 = 1$, $K_4 = 1$.

2. Band with coupling effects

When the width of the band gap is so small that the coupling effects become nonnegligible, we shall seek static breather-breather solutions of Eq. (26) on the form

$$\Phi(x, t) = A \text{sech}(\gamma x)e^{-i\omega_{s_1}t},$$
$$\Psi(x, t) = B \text{sech}(\gamma x)e^{-i\omega_{s_2}t}, \qquad (31)$$

where $\omega_{s_1} = \omega - \omega_{-\max}$. ω_{s_2}, γ, A, and B shall be defined by the solvability conditions.

When inserting Eq. (31) into Eq. (26), the solvability conditions yield

$$\gamma^2 = \frac{\omega_{s_1}}{P_1}, \qquad (32)$$

$$\omega_{s_2} = -\frac{\omega_{-\max}\omega_{s_1}}{\omega_{+\min}}, \qquad (33)$$

$$A = \pm i\sqrt{\frac{4\omega_{s_2}}{3Q_2} + \frac{2\omega_{s_1}}{3Q_1}}, \qquad (34)$$

$$B = \pm\sqrt{\frac{4\omega_{s_1}}{3Q_1} - \frac{2\omega_{s_2}}{3Q_2}}, \qquad (35)$$

and thereafter, the supratransmission threshold is given by

$$A_{th_{low_4}} = A_{th_{low_3}}\sqrt{1 - \frac{2}{3}\left(\frac{\omega_{+\min}^2 - \omega_{-\max}^2}{\omega_{+\min}^2}\right)}. \qquad (36)$$

The plotting of Eqs. (30) and (36) with respect to the driving frequency is displayed on Fig. 8, where we can see a good agreement with the numerical results of Eq. (30) for small mass ratio (acoustic mode behavior) and Eq. (36) for large mass ratio m/M (coupled mode behavior).

D. Effects of the mass of the driven particle on the supratransmission threshold

In this section, the order of the particles array $[M - m - M - m - M - \cdots]$ previously considered is switched into the diatomic lattice version $[m - M - m - M - \cdots]$, so that the driven particle (the first unit) has now the mass m.

1. Analytical analysis

The diatomic lattice consists on two sublattices having the masses m and M; the displacement of the nth particle of each sublattice are given by W_n and V_n, respectively. Since the first particle have the mass m, the seeking of threshold amplitude of supratransmission occurrence shall be done through the solution W of the envelope equation, on contrary to the lattice with a particle of mass M as first particle, for which the solution V is needed.

(1) In the upper forbidden band the decoupling ansatz procedure gives

$$W = \lambda_j \left[V + \sum_{l=1}^{4} b_{l,j} \frac{D^l}{l!} \partial_x^l V \right] + \mathcal{O}(D^5), \qquad (37)$$

which can be approximates at the first order as

$$W = \lambda V, \qquad (38)$$

where $\lambda = -1/\mu$. The supratransmission threshold which is the maximal amplitude of the static solution is then given by

$$B_{\text{th}_{up}} = |\lambda| A_{\text{th}_{up}}. \qquad (39)$$

(2) In the lower forbidden band, for a wide band gap, the decoupling ansatz procedure approximate at the first order gives

$$B = \sigma e^{ikD} A, \qquad (40)$$

where $\sigma = \frac{-\beta \pm \sqrt{\Delta}}{2\cos(kD)}$, $\Delta = \beta^2 + 4\frac{M}{m}\cos^2(kD)$, $\beta = \frac{M}{m} - 1$.

Around the limit $k = \pi/2D$ of the first Brillouin zone, we can do the approximation

$$kD = \frac{\pi}{2}(1 + \epsilon), \qquad (41)$$

with $\epsilon \ll 1$. Taking into account Eq. (41), we can write

$$\cos(kD) \approx -\frac{\pi \epsilon}{2},$$

$$e^{ikD} \approx -\frac{\pi \epsilon}{2} + i,$$

and for the acoustic mode

$$\sigma = \frac{\pi \epsilon}{2(1 - \mu)}. \qquad (42)$$

and thereafter, we derived the supratransmission threshold as

$$B_{\text{th}_{low1}} = \frac{\pi \epsilon \sqrt{1 + \frac{\epsilon^2 \pi^2}{2}}}{2(1 - \mu)} A_{\text{th}_{low1}}. \qquad (43)$$

2. Numerical study

The lattice is driven at that end by the same wave given in Sec. II. We plotted for the three couples (m, M) the supratransmission threshold as a function of driving frequency for

the upper (lower) forbidden band together with their analytical analogs Eq. (39) [Eq. (43)].

We can notice from Fig. 9 that the supratransmission threshold drastically changes when passing from a line with heavy-driven particle to a line with light-driven particle in both the two forbidden bands.

In lower forbidden band, a light-driven particle results in a decrease of the threshold in comparison with the case of heavy-driven particle, whereas in upper forbidden band we observe the opposite situation. Figure 9 also displays a good agreement, in both the two forbidden bands, between analytical thresholds for lattice with light-driven particle and their numerical analogs.

Our tentative attempt to identify an analytical threshold for the light-driven particle in the lower forbidden band with coupling effects yields findings that differ dramatically from the numerical simulations and are thus not provided in this study.

E. Bridging diatomic and monoatomic cases

At the limit $m = M$, the dispersion diagram of the diatomic lattice displays only one forbidden band which boundary, as well as that of the monoatomic lattice is known to be $\omega_{\max} = \sqrt{4/m}$ [30]. The location of the forbidden band, which is the same in the two cases, corresponds to the upper forbidden band of the diatomic lattice so that the valid threshold in the limit $m = M$ of the diatomic lattice shall be obtained by replacing M by m in Eq. (12). We can thus write this threshold on the form

$$A_{\text{th}_{up}} = \sqrt{\frac{m\omega(\omega - \omega_{\max})}{3K_4}}. \qquad (44)$$

The comparison between the analytical threshold Eq. (44) and those obtained for the monoatomic case for the small and large amplitudes [14,30]

$$A_{\text{th}_{mono1}} = \sqrt{\frac{m\omega^2 - 4K_2}{6K_4}}, \qquad (45)$$

$$A_{\text{th}_{mono2}} = \sqrt{\frac{16(m\omega^2 - 3K_2)}{81K_4}}, \qquad (46)$$

respectively, is displayed in Fig. 10(a). The thresholds estimated numerically are plotted as well. The simulations are performed for $m = M = 0.18$ and reveal for numerical estimations [Fig. 10(b)], a good agreement between the monoatomic case and the limit $m = M$ of the diatomic case.

For frequencies close to $\omega_{\max}$ (far from $\omega_{\max}$), a good agreement is observed between the limit $m = M$ [Eq. (44)] and the small amplitude [Eq. (45)] (and the large amplitude [Eq. (46)]) thresholds.

IV. DISCUSSION

Previously, in various diatomic lattices, the existence and stability of nonlinear static localized modes with frequencies in the forbidden frequency band gap were
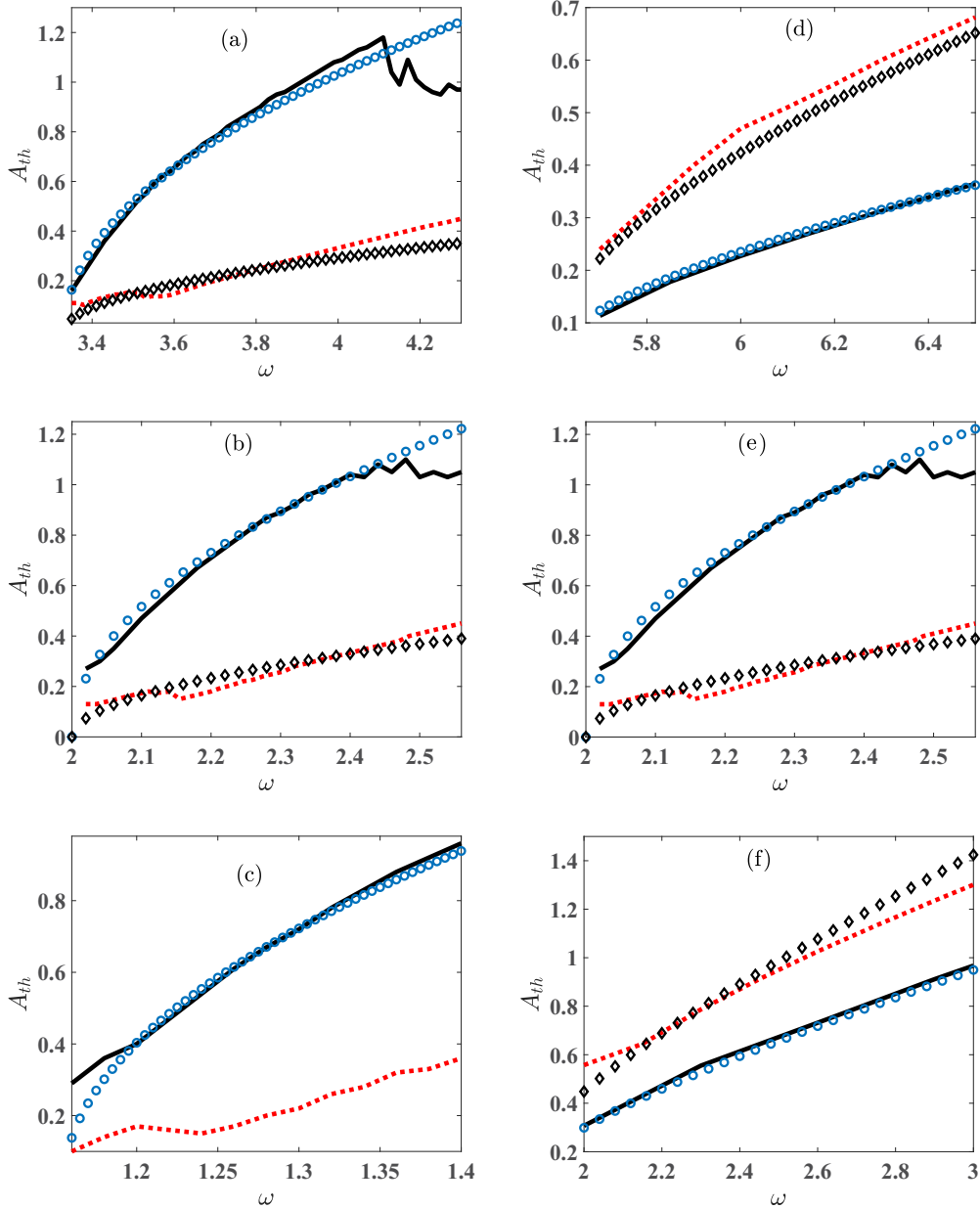
FIG. 9. Threshold amplitude versus the driving frequency for three couples (m, M): $(0.1, 0.18)$ (a) and (d); $(0.3, 0.5)$ (b) and (e); $(1, 1.5)$ (c) and (f). (a), (b), (c) for lower forbidden band; (d), (e), (f) for upper forbidden band. Black solid lines (red dashed lines) represent the numerical cases of heavy-driven particle (light-driven particle); and blue circles (black diamonds) their analytical analogs. $K_2 = 1$, $K_4 = 1$, $\epsilon = 0.08$.

investigated [6,9,15–17]. The present study demonstrates that these modes can propagate (or be supra-transmitted) along the lattice.

The nonlinear supratransmission phenomenon, previously observed in numerous monoatomic systems [18–21,24–26] has also been evidenced here in one-dimensional diatomic β-FPU lattice. In contrast to the monoatomic case [30,31], there are several forbidden frequency band gaps, thus making the investigation more difficult. As highlighted by Mekontchou *et al.* [23], only a few monoatomic models exhibit the supra-transmission at all the forbidden frequency bands [23]. This study advocates further investigations of other diatomic case models.

Similarly to what was found in previous studies [18–21,23–26,30,31], the phenomenon occurs when the amplitude of the sinusoidal excitation is greater than a certain value known as the threshold. In contrast to existing studies on di- and triatomic models [28,29], the supratransmission threshold has been derived analytically with acceptable accuracy by leveraging existing mathematical techniques for soliton investigation in nonlinear diatomic systems [32–36].

The nonlinear supratransmission in structures with more than one elements inside the unit cells (induced respectively by force-constant difference and two masses of two kinds of particles) where studied by Zhang *et al.* [28] as well as Wu and
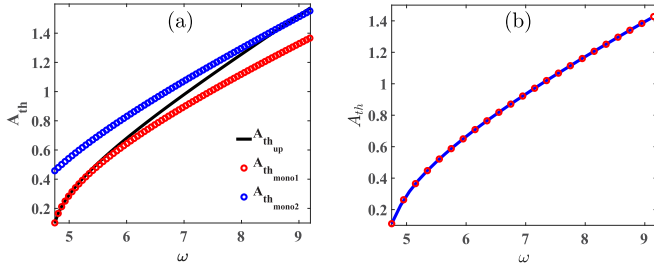
FIG. 10. Threshold amplitude versus driving frequency, for monoatomic case and for the limit $m = M$ of diatomic case. (a) for analytical thresholds and (b) for numerical simulations, $K_2 = 1$, $K_4 = 1$.

Wang [29]. In contrast to the present study, Zhang *et al.* [28] based their conclusion solely on numerical simulations. The authors Wu and Wang [29] somehow overlooked the effect of the mass ratio which is proven to be detrimental for the onset of supratransmission in the present study; noticed via the increases of the threshold value.

Due to the coupling of motion of odd-even (of masses m-M) positioned particles of the diatomic β-FPU, it is found that the rotating wave approximation used in monoatomic FPU [30] is not efficient enough to derive the threshold of supratransmission occurrence. Our attempt to use the same method did not provide analytical results closer to the numerical exact threshold. Nevertheless, the decoupling ansatz method [32,33,33–36], is proven to be a useful tool for the derivation of envelope equation which provide, in the upper forbidden band a threshold which is in good agreement with the numerical one in the same gap. Although the threshold derived in the upper forbidden band explicitly depends on the mass ratio μ, its validity and its accurateness is preserved for all value of μ.

The threshold obtained for the lower forbidden band through the continuum form of the decoupling ansatz method [33] was not in agreement with the numerical simulations. This is due to the fact that at the boundary of the lower forbidden band on the dispersion law, located at $k = \pi/2D$, the long wavelength limit, valid for $k = 0$ (boundary of the upper forbidden band) becomes less accurate. Fortunately, a more general form, valid for arbitrary wavelength exists for the decoupling ansatz [34]. This form provides an analytical threshold, which is in good agreement with the numerical results. It is also easy to check that for $k = 0$, we obtain, through that general form the results of Sec. II A. Moreover, it can be noticed that this threshold is not an explicit function of mass ratio μ and is in good agreement with numerical results for small values of this ratio ($\mu \leqslant 60\%$). This accordance confirms the hypothesis of acoustic mode vibration in lower forbidden band and the decoupling between the optical and the acoustic modes. However, for values of the driving frequency sufficiently close to $\omega_{+\min}$, the coupling effects become very significant and result in a decreasing of the threshold with the increase of the driving frequency as we can observe in Figs. 7(a) and 7(b), 8(a) and 8(b), and 9(a) and 9(b). In other words, the anomalous observed through the decreasing of the threshold are due to the coupling effects between the optical and acoustic mode; this observation is confirmed by the case

of narrow band gap where the thresholds obtained when the coupling is taking into account are globally lower than those obtained without coupling effects.

For large values of mass ratio ($\mu > 60\%$), the coupling between acoustic and optical modes in the lower forbidden band, which has been previously investigated by Hu *et al.* [37] has been considered to derive the supratransmission threshold, since the threshold Eq. (19) is no longer in accordance with numerical results. The threshold Eq. (36), derived when taking into account the coupling between the two modes, displays an explicit dependence on the frequency of these two modes, and a good agreement with the numerical results proves the actual presence of a coupling which strength increases with the increasing of the mass ratio. Moreover, we observe that using this coupling mode procedure, we can also derive, as one of the results, the same threshold Eq. (30) obtained when neglecting the coupling between the two modes.

A surprising and very interesting aspect of this work is the changing of the supratransmission threshold when switching the order of particles. In fact, this switch does not affect the physical properties of the lattice (apart of the mass of the driven particle) but is found relevant for the study of the supratransmission phenomenon in diatomic lattices. The choice of the driven particle (light or heavy) is thus crucial for the study of supratransmission and more generally for the study of dynamic of diatomic lattices under external excitation. The consequences of such a behavior on real physical systems modeled by diatomic lattice could be very interesting.

The comparison of our results with the existing theory has been done by studying the limit case $m = M$ of the diatomic lattice. Overall, the analytical and numerical results are consistent with monoatomic FPU [30]. The two thresholds found in Ref. [30] (for low and large amplitude) are in agreement, the first with the low amplitude and the second with the large amplitude part of the limit ($m = M$) case of the diatomic threshold obtained in the upper forbidden band.

The convergence and the accurateness (in comparison with the numerical analogs) of analytical procedures used in this paper to derive supratransmission thresholds in each forbidden band are displayed in Table I.

V. CONCLUSION

In this study, it is demonstrated that the supratransmission in diatomic chain can occur in the upper and lower forbidden bands, and the threshold amplitudes above which the phenomenon occurs have been derived for both forbidden bands numerically and analytically. The accurateness of the numerical and analytical methods is established by estimating the threshold as a function of driving amplitude for several values of the ratio m/M and also with the study of the limit case $m = M$ which shows a good agreement with the existing theory. Furthermore, we found in the two forbidden bands a different supratransmission threshold when switching the order of particles from a chain with a heavy first particle to a chain with a light first particle. This peculiar behavior as well as the dependence in the lower forbidden band of the supratransmission on band width show the asymmetric character of diatomic lattices and the necessity to consider several analytical approaches when dealing with such lattices.

TABLE I. Comparison and accurateness of analytical procedures. The parameters μ and k are the mass-ratio (m/M) and wave vector, respectively. $\sqrt{}$: applicable technic with accurate results, ✗: applicable technic but does not track closely the numerical results, N.A.: not applicable.

Analytical technics	Upper forbidden band for $\mu \leqslant 60\%$	Upper forbidden band for $\mu > 60\%$	Forbidden band between acoustic and optical modes for $\mu \leqslant 60\%$	Forbidden band between acoustic and optical modes for $\mu > 60\%$
Decoupling ansatz with $k \to 0$	$\sqrt{}$	$\sqrt{}$	N.A.	N.A.
Decoupling ansatz with k arbitrary	N.A.	N.A.	$\sqrt{}$	✗
Coupled modes	N.A.	N.A.	$\sqrt{}$	$\sqrt{}$

[1] M. I. Hussein, M. J. Leamy, and M. Ruzzene, Dynamics of phononic materials and structures: Historical origins, recent progress, and future outlook, Appl. Mech. Rev. **66**, 040802 (2014).

[2] S. Aubry, Discrete breathers: Localization and transfer of energy in discrete Hamiltonian nonlinear systems, Physica D **216**, 1 (2006).

[3] A. M. Morgante, M. Johansson, G. Kopidakis, and S. Aubry, Standing wave instabilities in a chain of nonlinear coupled oscillators, Physica D **162**, 53 (2002).

[4] P. G. Kevrekidis, *The Discrete Nonlinear Schrödinger Equation: Mathematical Analysis, Numerical Computations and Physical Perspectives* (Springer, Berlin, 2009).

[5] S. Flach and A. V. Gorbach, Discrete breathers—Advances in theory and applications, Phys. Rep. **467**, 1 (2008).

[6] N. Boechler, G. Theocharis, S. Job, P. G. Kevrekidis, M. A. Porter, and C. Daraio, Discrete breathers in one-dimensional diatomic granular crystals, Phys. Rev. Lett. **104**, 244302 (2010).

[7] M. A. Porter, C. Daraio, E. B. Herbold, I. Szelengowicz, and P. G. Kevrekidis, Highly nonlinear solitary waves in periodic dimer granular chains, Phys. Rev. E **77**, 015601(R) (2008).

[8] S.-Y. Lou and G. Huang, Experimental study of the solitons in nonlinear diatomic macro-lattice, Mod. Phys. Lett. B **09**, 1231 (1995).

[9] F. Palmero, L. Q. English, X.-L. Chen, W. Li, J. Cuevas-Maraver, and P. G. Kevrekidis, Experimental and numerical observation of dark and bright breathers in the band gap of a diatomic electrical lattice, Phys. Rev. E **99**, 032206 (2019).

[10] A. K. Farota and M. M. Faye, Experimental study of the Fermi-Pasta-Ulam recurrence in a bi-modal electrical transmission line, Phys. Scr. **88**, 055802 (2013).

[11] T. C. Kofané, B. Michaux, and M. Remoissenet, Theoretical and experimental studies of diatomic lattice solitons using an electrical transmission line, J. Phys. C: Solid State Phys. **21**, 1395 (1988).

[12] *The Fermi-Pasta-Ulam Problem*, edited by G. Gallavotti (Springer, Berlin, 2008).

[13] M. Remoissenet, *Waves Called Solitons* (Springer, Berlin, 1999).

[14] L. Brillouin, *Periodic Structure: Electronic Filters and Crystal Lattices*, 1st ed. (McGraw-Hill, New York, NY, 1946).

[15] P. Maniadis, A. V. Zolotaryuk, and G. P. Tsironis, Existence and stability of discrete gap breathers in a diatomic Fermi-Pasta-Ulam chain, Phys. Rev. E **67**, 046612 (2003).

[16] A. V. Gorbach and M. Johansson, Discrete gap breathers in a diatomic Klein-Gordon chain: Stability and mobility, Phys. Rev. E **67**, 066608 (2003).

[17] K. Yoshimura, Existence and stability of discrete breathers in diatomic Fermi-Pasta-Ulam type lattices, Nonlinearity **24**, 293 (2011).

[18] F. Geniet and J. Leon, Energy transmission in the forbidden band gap of a nonlinear chain, Phys. Rev. Lett. **89**, 134102 (2002).

[19] T. V. Koon, P. Marquié, and P. T. Dinda, Experimental observation of the generation of cut-off solitons in a discrete LC nonlinear electrical line, Phys. Rev. E **90**, 052901 (2014).

[20] R. Khomeriki, Nonlinear band gap transmission in optical waveguide arrays, Phys. Rev. Lett. **92**, 063905 (2004).

[21] B. Yousefzadeh and A. S. Phani, Supratransmission in a disordered nonlinear periodic structure, J. Sound Vib. **380**, 242 (2016).

[22] F. Kenmogne, G. B. Ndombou, D. Yemélé, and A. Fomethe, Nonlinear supratransmission in a discrete nonlinear electrical transmission line: Modulated gap peak solitons, Chaos Solitons Fractals **75**, 263 (2015).

[23] M. Mekontchou Foudjio, F. Thomas Ndjomatchoua, C. L. Gninzanlong, and C. Tchawoua, Collective escape and supratransmission phenomena in a nonlinear oscillators chain, Chaos **30**, 123122 (2020).

[24] J. E. Macías-Díaz, Numerical study of the transmission of energy in discrete arrays of sine-Gordon equations in two space dimensions, Phys. Rev. E **77**, 016602 (2008).

[25] M. Malishava and R. Khomeriki, All-phononic digital transistor on the basis of gap-soliton dynamics in an anharmonic oscillator ladder, Phys. Rev. Lett. **115**, 104301 (2015).

[26] M. Malishava, All-phononic amplification in coupled cantilever arrays based on gap soliton dynamics, Phys. Rev. E **95**, 022203 (2017).

[27] A. K. Kuitche, A. B. Togueu Motcheyo, T. Kanaa, and C. Tchawoua, Supratransmission in transversely connected nonlinear pendulum pairs, Chaos Solitons Fractals **160**, 112196 (2022).

[28] Q. Zhang, H. Fang, and J. Xu, Programmable stopbands and supratransmission effects in a stacked Miura-origami metastructure, Phys. Rev. E **101**, 042206 (2020).

[29] Z. Wu and K. W. Wang, On the wave propagation analysis and supratransmission prediction of a metastable modular metastructure for nonreciprocal energy transmission, J. Sound Vib. **458**, 389 (2019).

[30] R. Khomeriki, S. Lepri, and S. Ruffo, Nonlinear supratransmission and bistability in the Fermi-Pasta-Ulam model, Phys. Rev. E **70**, 066626 (2004).

[31] J. E. Macías-Díaz and A. Bountis, Supratransmission in β-Fermi-Pasta-Ulam chains with different ranges of interactions, Commun. Nonlinear Sci. Numer. Simul. **63**, 307 (2018).

[32] P. C. Dash and K. Patnaik, Solitons in nonlinear diatomic lattices, Prog. Theor. Phys. **65**, 1526 (1981).

[33] S. Pnevmatikos, M. Remoissenet, and N. Flytzanis, Propagation of acoustic and optical solitons in nonlinear diatomic chains, J. Phys. C: Solid State Phys. **16**, L305 (1983).

[34] S. Pnevmatikos, N. Flytzanis, and M. Remoissenet, Soliton dynamics of nonlinear diatomic lattices, Phys. Rev. B **33**, 2308 (1986).

[35] *Solitons and Condensed Matter Physics*, edited by A. R. Bishop and T. Schneider (Springer, Berlin, 1978).

[36] C. Tchawoua, T. C. Kofane, and A. S. Bokosah, Dynamics of solitary waves in diatomic chains with long-range Kac-Baker interactions, J. Phys. A: Math. Gen. **26**, 6477 (1993).

[37] B. Hu, G. Huang, and M. G. Velarde, Dynamics of coupled gap solitons in diatomic lattices with cubic and quartic nonlinearities, Phys. Rev. E **62**, 2827 (2000).

[38] M. Johansson, G. Kopidakis, S. Lepri, and S. Aubry, Transmission thresholds in time-periodically driven nonlinear disordered systems, Europhys. Lett. **86**, 10009 (2009).

[39] P. Maniadis, G. Kopidakis, and S. Aubry, Energy dissipation threshold and self-induced transparency in systems with discrete breathers, Physica D **216**, 121 (2006).